Bull Eng Geol Environ (2016) 75:1597–1607
DOI 10.1007/s10064-015-0816-8

ORIGINAL PAPER

Influence of tunnel wall roughness and localized stress concentrations on the initiation of brittle spalling

Songfeng Guo[1,2] · Shengwen Qi[1] · Ming Cai[3]

Received: 2 March 2015 / Accepted: 11 November 2015 / Published online: 24 November 2015

Abstract Brittle failure of massive hard rocks occurs when the stress near the excavation reaches the in situ strength. After reviewing published papers, we found that two approaches, one using $UCS^{ci}_{field} \approx 0.45\ UCS_{lab}$ and the other using $UCS^{cd}_{field} \approx 0.8\ UCS_{lab}$, have been used to estimate the in situ strength of massive rock, where UCS_{field} and UCS_{lab} are the field and laboratory uniaxial compressive strengths, respectively, and the superscripts denote UCS_{field} defined by the crack damage stress or crack initiation stress. In this study, a continuum model considering the "as built profile" was constructed to simulate brittle rock failure in two orthogonal tunnels in the 420 level of Atomic Energy of Canada Limited's (AECL's) Underground Research Laboratory. Results obtained from the simulation with in situ strength at UCS^{cd}_{field} seem to capture actual rock conditions better than that with the in situ strength at UCS^{ci}_{field}. Opening wall roughness has a great influence on the brittle failure of massive hard rocks. It was found that compared with the smooth boundary condition, stress can concentrate around the rough boundary and the induced tensile stress driven by compressive stress loading can promote rock spalling failure. If the opening roughness is overlooked, the field uniaxial compressive strength of UCS_{field} will be underestimated.

Keywords Brittle rock failure · In situ rock strength · Stress concentration · Spalling

Introduction

It is known that the tunnel instability and failure modes are strongly influenced by in situ stresses and rock mass strength (Hoek and Brown 1980). If brittle failure occurs around the opening perimeter, the stress near the excavation boundary must have reached the in situ rock mass strength. One interesting observation is that in some stress analyses using elastic models for tunnels with simplified smooth tunnel walls, the field stress did not reach the rock strength determined in the laboratory, but brittle failures occurred in these tunnels (Martin 1993, 1997; Martin et al. 1999; Fang and Harrison 2002).

Much work had been conducted to study the problems of in situ rock strength, and some viewpoints have been proposed. In sparsely jointed rock masses, the in situ rock strength is weakened compared to that obtained from laboratory tests because of factors such as the scale effect (Hoek and Brown 1980; Lockner 1995; Martin et al. 2011), loading rate (Laigle 2006), heterogeneity (Cai 2011) or stress rotation (Eberhardt 2001). Research has shown that the brittle rock failure under compression is progressive, and the process can be summarized into five stages: crack closure, linear elastic deformation, crack initiation and stable crack growth, crack damage and unstable crack

✉ Shengwen Qi
qishengwen@mail.iggcas.ac.cn

Songfeng Guo
guosongfeng@mail.iggcas.ac.cn

Ming Cai
mcai@laurentian.ca

[1] Key Lab of Shale Gas and Geological Engineering, Institute of Geology and Geophysics, Chinese Academy of Sciences, No. 19 Beituchengxilu, Chaoyang District, Beijing 100029, China

[2] University of Chinese Academy of Sciences, Beijing 100049, China

[3] Bharti School of Engineering, Laurentian University, Sudbury, ON P3E 2C6, Canada

growth, and post peak (Bieniawski 1967; Martin 1997; Eberhardt et al. 1999; Cai et al. 2004). Three key stress levels, i.e., crack initiation stress (σ_{ci}), crack damage stress (σ_{cd}) and peak strength (σ_f), can be identified. The crack initiation stress in low-porosity brittle rocks is between 0.3 and 0.5 times the σ_f under low confinement (Brace et al. 1966; Martin 1997; Diederichs et al. 2004; Nicksiar and Martin 2013). The crack damage stress, which represents the long-term strength of the rock, is about 0.7–0.8 times the peak stress (Lockner et al. 1992; Martin and Chandler 1994).

Based on failure observation in the field and elastic stress analysis of a URL (underground research laboratory) Mine-by tunnel model with a simplified smooth boundary, Martin (1997) stated the in situ rock strength around the excavations can be defined by the damage initiation threshold as (0.3–0.5) UCS (uniaxial compression strength) of rocks, and some researchers adopted a similar reduction for in situ strength in their studies (e.g., Read et al. 1998; Hajiabdolmajid et al. 2002). Diederichs (2007) proposed a combined damage initiation and spalling limit approach in which the damage initiation stress defines the lower bound strength at low confining stress, the crack damage stress defines the upper bound strength at higher confining stress, and a spalling limit defines the transition. This approach was also suggested by Kaiser et al. (2000, 2011), who named it an 'S'-shaped strength envelope. Read et al. (1998) and Read (2004) indicated that the stress near the excavation boundary is highly influenced by the tunnel shape. Cai and Kaiser (2014) considered the rough boundary of the Mine-by tunnel in their analysis and stated that the stress can concentrate around the rough boundary and actual in situ rock strength near the tunnel wall can be estimated by the crack damage stress reached in the laboratory rather than the crack initiation stress. Because there are diverse opinions about the in situ rock strength, more field case studies are needed to seek the truth about the in situ rock strength.

This article describes the simulation of the brittle failure of two orthogonal tunnels in the 420 level of AECL's underground research laboratory. In the study, the in situ rock strengths defined by the crack initiation stress ($UCS^{ci}_{field} \approx 0.45\ UCS_{lab}$) and the crack damage stress ($UCS^{cd}_{field} \approx 0.8\ UCS_{lab}$) are used respectively to clarify the stress state and rock strength in the field.

Brittle rock failure in tunnels in the underground research laboratory, Canada

A well-known case of brittle rock failure is the notch brittle failure occurring in the Mine-by tunnel at URL, located in Manitoba, Canada. The tunnel was situated within massive Lac du Bonnet granite, which is representative of many granitic intrusions of the Precambrian Canadian Shield (Everitt et al. 1990). The massive, medium- to coarse-grained porphyritic granite is relatively uniform in texture and composition over the batholith, although locally it displays subhorizontally. According to the laboratory data, the Young's modulus, Poisson ratio, uniaxial compressive strength and uniaxial tensile strength (Brazilian test) are about 69 GPa, 0.26, 220 and 13.25 MPa, respectively (Martin 1993). Two major faults dip about 25–30 southeast in the URL excavation area, i.e., fracture zones 2 and 3 in Fig. 1, (Martin 1997). Joints are developed at the shallow layer and stops at a depth of about 220 m. The Mine-by experiment tunnel is located at a depth of 420 m (420 level), about 200 m below the jointed rock mass. Only six fractures with a trace length less than 1.5 m encountered during the tunnel excavation and boreholes drilled to depths of over 1000 m show that the massive granite persists with depth. Hence, it can be concluded that the Mine-by tunnel was excavated in massive, sparsely fractured granite (Martin 1997). According to the in situ stress data and back analysis, the maximum, intermediate and minimum principal stresses are $\sigma_1 = 60$, $\sigma_2 = 45$ and $\sigma_3 = 11$ MPa, respectively; see Fig. 2a (Martin 1990, 1997). The tunnel axis is nearly parallel to the intermediate stress direction. Initially, researchers used a simplified smooth tunnel model to conduct stress analysis and reached the conclusion that the maximum tangential stress at the smooth tunnel wall is about 169 MPa according to the elastic theory. This stress is much smaller than 220 MPa, the average UCS of the rock from the laboratory test (Martin 1993). Despite the fact that the excavation for the Mine-by tunnel was carried out using a careful perimeter line drilling and mechanical breaking excavation method to avoid blasting damage (Martin 1997), spalling failure leading to notch formation was observed [see the profile of the Mine-by tunnel (room 415) in Fig. 2b]. A similar type of spalling failure to that observed in the Mine-by tunnel was found in other tunnels excavated parallel or near parallel to the intermediate stress, such as in room 405 (Fig. 2b). However, no obvious notch-shaped failures were observed in tunnels that were oriented orthogonally to the Mine-by tunnel or in the direction sub-parallel to the maximum principal stress, such as in room 413 (Fig. 2b). Note that rooms 405 and 413 were excavated using the conventional drill-and-blast technique. To minimize blasting-induced damage, the smooth perimeter blasting technique was used.

Researchers have studied the rock failure in the Mine-by tunnel, and some of them have reproduced the V-shaped failure in their numerical modeling (Cai and Kaiser 2014; Hajiabdolmajid et al. 2002; Diederichs 2007). Different from the Mine-by Tunnel, the designed tunnel profiles of rooms 405 and 413 were not circular, and the as-built

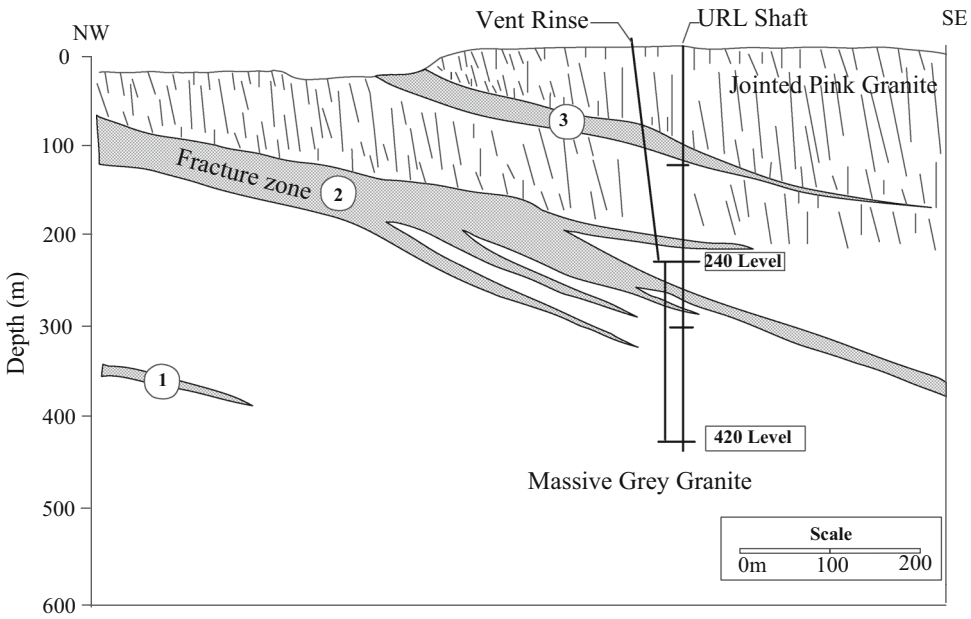

Fig. 1 Northwest–southeast geological section through URL (Martin 1997)

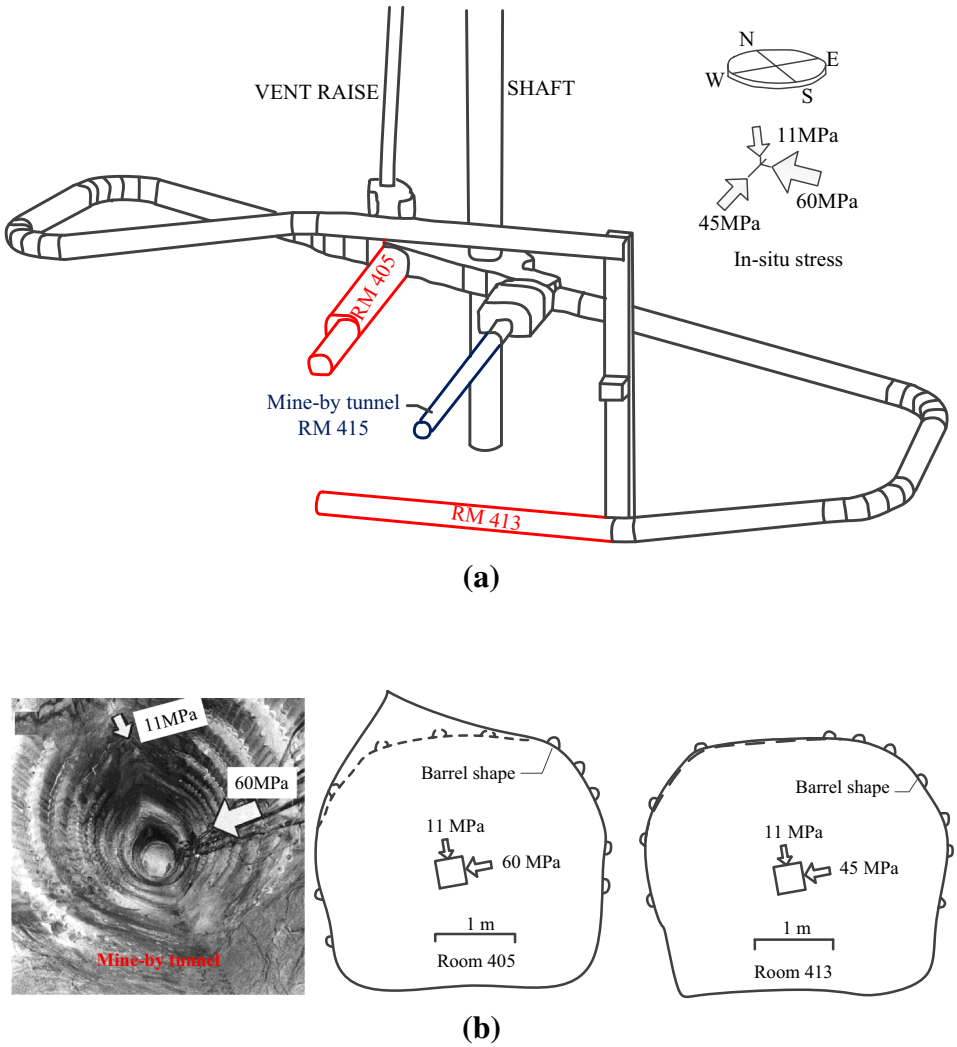

Fig. 2 **a** Tunnel layout in the 420 level of URL; **b** the profiles of three studied tunnels. The *solid lines* represent the final profile, while the *dashed lines* represent the original profiles of rooms 405 and 413 [modified from Martin (1993)]

boundaries were very irregular because of the full-face drill-and-blast excavation technique used. The good quality of the smooth blasting was evident because many half barrels could be seen on the walls (see Fig. 2b). Martin (1993) conducted stress analyses for the two orthogonal tunnels and concluded that the stress around the perimeter of the tunnels was much lower than the uniaxial compressive strength of the granite obtained in the laboratory. It should be noted that the profiles of the models in the analysis were simplified as smooth tunnel walls, and the stress alteration due to rough tunnel walls was ignored. In the following section, we carry out numerical studies on the two tunnels (rooms 405 and 413) to investigate the in situ strength of brittle rocks.

Modeling the spalling failure in rooms 405 and 413 at URL

Numerical models were built based on the as-built profiles of rooms 405 and 413 shown in Fig. 2b using FLAC^{3D}, and a plane with one unit thickness perpendicular to the tunnel axis is cut off and shown in Fig. 3. Half barrels on the perimeter of the tunnels were carefully modeled. The outer boundary of the models was five times the tunnel height. A very fine mesh with over 16,000 six-node elements, i.e., wedge elements in FLAC^{3D}, was used to increase the stress analysis accuracy. Initially, the 3D in situ stress was applied at the corresponding boundary, and the program was executed until balance was achieved. After that, the tunnel was excavated with model null command as suggested by the manual of FLAC^{3D}.

Two sets of strength parameters were adopted by Hajiabdolmajid et al. (2002) and Cai and Kaiser (2014) to study the Mine-by tunnel notch failure. Coincidently, the in situ rock strength used by Hajiabdolmajid et al. (2002) and Cai and Kaiser (2014) were roughly the same as the crack initiation stress and crack damage stress, respectively. In other words, the uniaxial compressive strength was 179 MPa (about 0.8 UCS_{lab}) in Cai and Kaiser (2014) and 100 MPa (about 0.45 UCS_{lab}) in Hajiabdolmajid et al. (2002). In this simulation, both strength parameters (Table 1) were used and the results compared. The deformation parameters used in the previous two papers were also applied, and the tensile strength was adopted as 13.4 MPa according to the results of the Brazilian tests summarized in (Martin 1993). It was noticed that the elastic modulus (E) and Poisson's ratio (υ) were not fully in accord with the laboratory test results of Martin (1993). Nevertheless, as is known, deformation parameters play a secondary role in the rock failure compared with the strength parameters, so for comparison we adopted all the parameters fully according to those of Hajiabdoamajid et al. (2002) and Cai and Kaiser (2014), respectively, in the simulation of this section. In other sections, we adopted the deformation parameters after the laboratory test results of Martin (1993), as mentioned in the previous part. A strength model of cohesion loss and friction mobilization was used in the simulation, in which the parameters of the Mohr-Coulomb strength criterion are not constant during the failure, i.e., the cohesion is gradually decreased, the friction angle is gradually increased, and the tensile strength disappears when the plastic strain increases. Some researchers stated that the frictional strength component is only mobilized after a significant amount of the rock's cohesional strength has been lost in brittle rocks (Martin and Chandler 1994; Hajiabdolmajid et al. 2002). Therefore, the initial friction angle should be valued as 0° and mobilized after the cohesional strength starts to be lost [see that of Hajiabdoamajid et al. (2002) in Table 1]. The

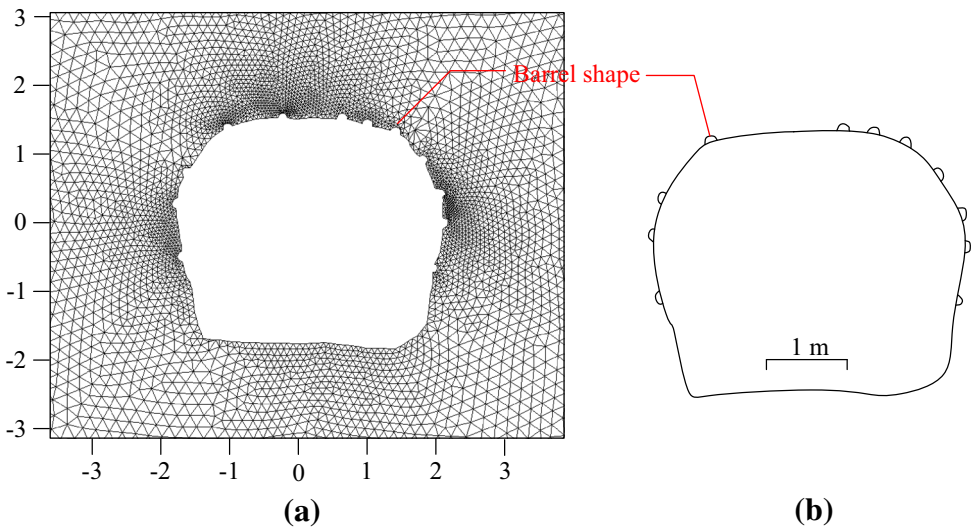

Fig. 3 **a** FLAC^{3D} model with as-built tunnel profile **b** to represent rooms 405 and 413

Table 1 Parameters adopted in the model with the as-built tunnel profile

	UCS^{ci}_{field} (about 0.45 UCS_{lab}) (Hajiabdolmajid et al. 2002)					UCS^{cd}_{field} (about 0.8 UCS_{lab}) (Cai and Kaiser 2014)				
	c (MPa)	ϕ (°)	E (GPa)	υ	σ_t (MPa)	c (MPa)	ϕ (°)	E (GPa)	υ	σ_t (MPa)
Initial	50	0	60	0.2	13.4	59	22	60	0.3	13.4
Residual	15	48	60	0.2	0	0.1	45	60	0.3	0
Plastic strain	0.002	0.005	N/A	N/A	0	0	0	N/A	N/A	0

strength model has been proved to be suitable for the brittle rock mass at depth (Martin 1997; Hajiabdolmajid et al. 2002; Guo et al. 2013). Note that Cai and Kaiser (2014) use the elastic-brittle model in their simulation, which means the residual strength is reached when failure occurs.

The spalling failure in room 405 was modeled first. The principal stresses of $\sigma_1 = 60$ MPa, $\sigma_2 = 45$ MPa and $\sigma_3 = 11$ MPa were used, and the orientations of σ_1 and σ_3 can be seen in Fig. 4. In situ stress was applied first to the model. Tunnel excavation was conducted in steps following the method used in Cai and Kaiser (2014).

The simulation results are shown in Fig. 4. If the set of strength parameters with UCS^{ci}_{field} is used, rock failure occurs both in the roof and on the floor (Fig. 4a). However, if the set of strength parameters with UCS^{cd}_{field} is used, rock failure occurs mostly in the roof and very little on the floor (Fig. 4b). The simulated failure zone in Fig. 4a is much greater than that observed in the field indicated by the dashed line. The failure zone in Fig. 4b is closer to the actual field condition. The result implies that the approach of using $UCS^{ci}_{field} = 0.45$ UCS_{lab} may underestimate the in situ strength of brittle rocks.

Next, rock failure in room 413 was modeled using the two sets of model parameters shown in Table 1. For room 413, the maximum in-plane in situ stress is $\sigma_2 = 45$ MPa. The modeling result of the failure zone using the model parameters of Hajiabdolmajid et al. (2002) is presented in Fig. 5a. It can be seen that the notch failures occurred in the roof and on the floor, which is different from the condition observed in the field. On the other hand, the modeling result using the model parameters of Cai and Kaiser (2014) shows that failure occurred just at the one half barrel location in the roof (Fig. 5b), which matches the field record (Martin 1993). It is confirmed that approach of using $UCS^{cd}_{field} = 0.8$ UCS_{lab} to approximate the in situ strength is more suitable than that using $UCS^{ci}_{field} = 0.45$ UCS_{lab}, which is in agreement with that stated in Cai and Kaiser (2014).

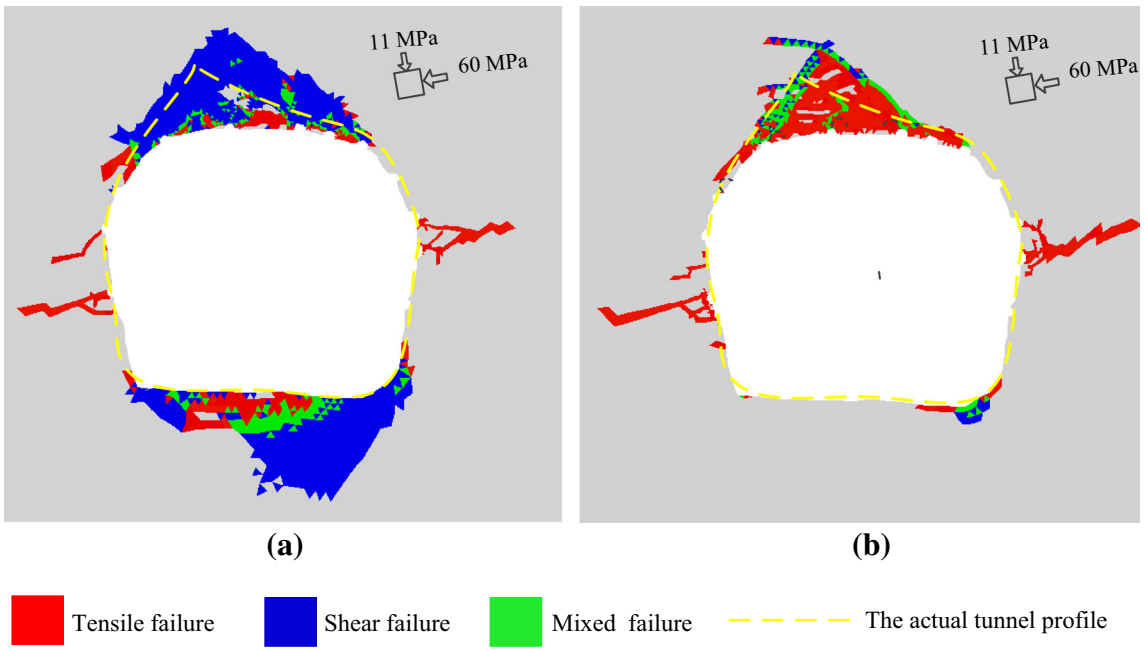

Fig. 4 Calculated failure shapes in room 405 based on a model with the as-built profile: **a** model parameters based on Hajiabdolmajid et al. (2002); **b** model parameters based on Cai and Kaiser (2014)

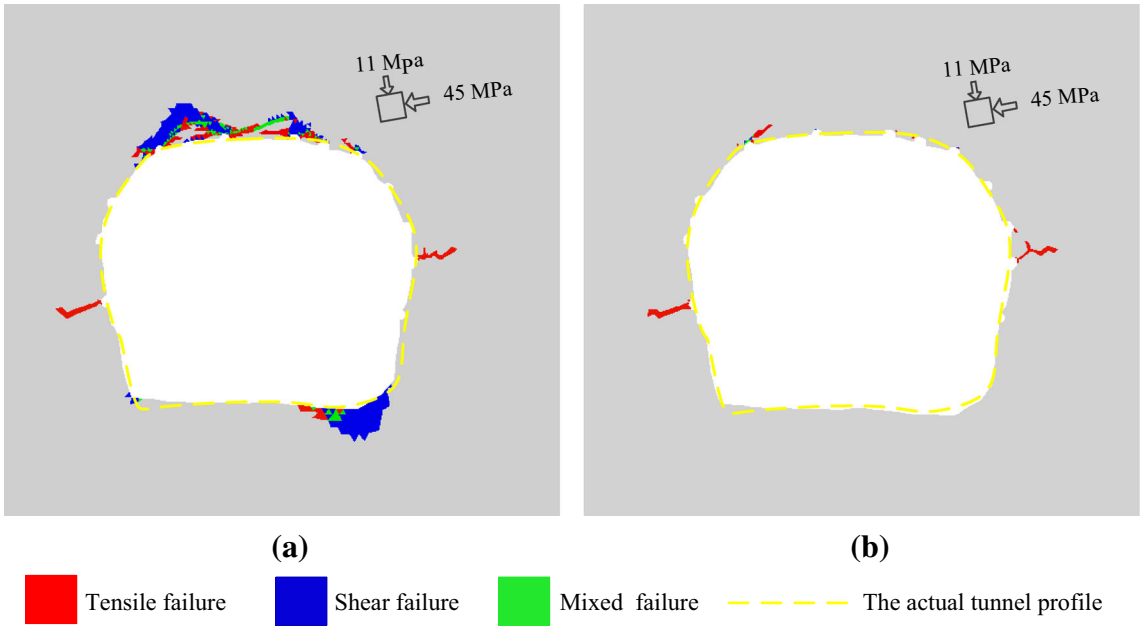

Fig. 5 Calculated failure shapes in room 405 based on a model with the as-built profile: **a** model parameters based on Hajiabdolmajid et al. (2002); **b** model parameters based on Cai and Kaiser (2014)

It can be inferred from the results shown above that the irregular boundary of the tunnel should not be ignored in rock failure analysis. It seems that the in situ strength was underestimated in some previous studies in which the smooth boundary was used. The essence is that an unexpected near-field stress concentration rather than in situ strength reduction is needed to capture rock failure in the field. In this way, the modeling exercise honors the physics and mechanics in the field and minimizes human fudge factors.

It is shown that the process of notch failure is progressive, i.e., the stress becomes highly concentrated because of the rough boundary of the tunnels in the field, and failure initiates at these locations where the stress reaches the in situ rock strength and grows progressively as the tunnel face advances until the final failure zone is formed. We also notice that tensile failure always initiates first, followed by the shear failure (Fig. 6).

Discussion

The comparison of results shown above indicates that the rough boundary of a tunnel influences rock failure and ignoring this would underestimate the in situ strength of a rock mass. In this section, we discuss the influence of the roughness of the tunnel boundary on the stress redistribution around the tunnel perimeter and its implication for the stress-induced rock failure.

To study the influence of tunnel boundary roughness on stress redistribution, a circular tunnel with a 3.5-m diameter is considered. Regular barrels aligned in the perimeter, similar to those in the Mine-by tunnel shown in Fig. 2b, are modeled. Series of tunnel models with different boundary roughnesses, represented by various curvatures of the barrels, are built, indicated by the ratio of a/L, where a is the chord height and L is the half chord length (Fig. 7). The number of barrels is fixed as 72, and a is varied from 0 to L. The relation between a/L and the stress concentration factors (SCF) represented as the maximum principal stress around the tunnel boundary in the rough boundary model to the maximum principal stress in the smooth boundary model $\sigma_{max}/\sigma_{max0}$ and the minimum principal stress to the maximum principal stress in the rough boundary model $\sigma_{min}/\sigma_{max}$, are shown in Fig. 7. It can be seen that when $a/L = 1$, the boundaries of the tunnel are aligned with perfect half barrels. When $a/L = 0$, the tunnel boundary is smooth. A linear elastic model with an elastic modulus of 69 GPa and Poisson's ratio 0.26 is used to obtain the stress data. Figure 7 shows that the maximum SCF is 1.4 for a very rough tunnel boundary, which means that the maximum compressive stress can be elevated 40 % higher than that from a smooth tunnel wall case to initiate rock failure. Tensile stress was noticed at the tunnel perimeter in the rough model once a/L was larger than 0.26, and the rougher the tunnel, the larger the tensile stress (see red line in Fig. 7). The stress distribution in the rough model ($a/L = 1$) and smooth model ($a/L = 0$) is also shown in

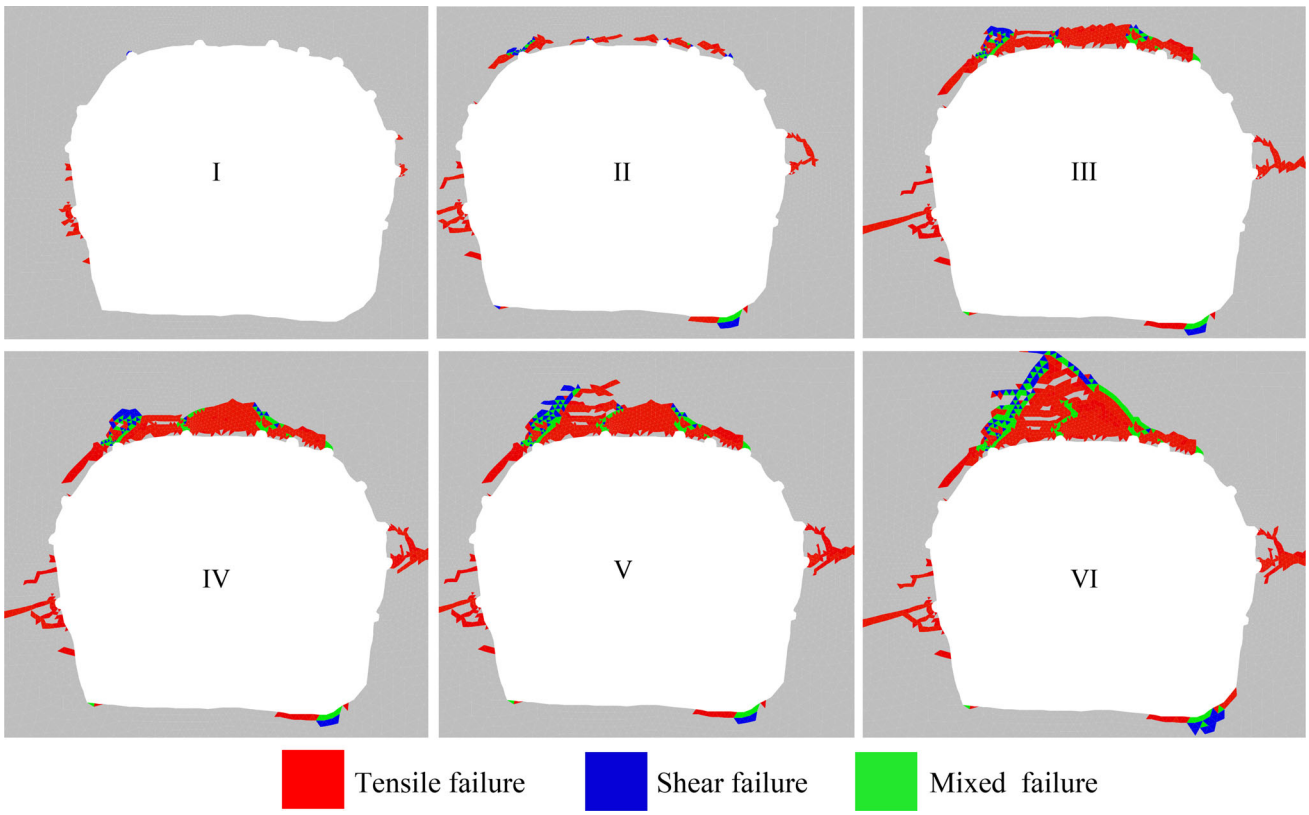

Fig. 6 Progressive failure of room 405 with model parameters based on Cai and Kaiser (2014)

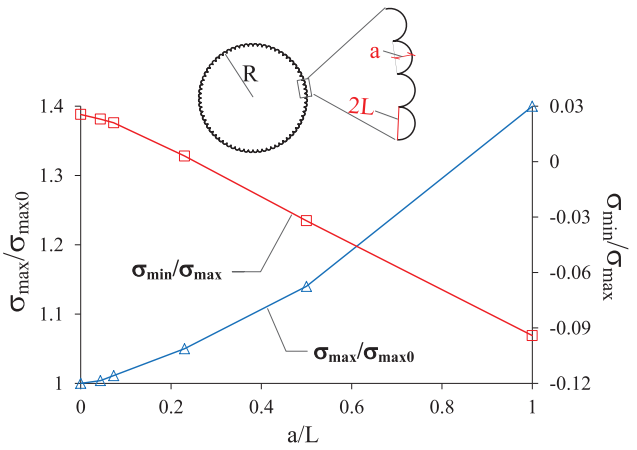

Fig. 7 The stress disturbance induced by tunnel boundary roughness

Fig. 8. It can be seen that the stresses are strongly nonuniform in the rough model; the compressive stress concentrates at the concave area and tensile stress concentrates at the convex area at the tunnel wall; see Fig. 8a, b. However, in the smooth model, the stress is more uniform; see Fig. 8c, d. It can also be seen that tensile failure dominates at the initiation of damage, followed by shear failure initiation and progression (see Fig. 6).

It can be seen from above that the boundary profile has great influence on the stress distribution and then the rock mass failure. It was well known that the smooth boundary profile only consists of concave shapes, and the rough boundary profile consists of a series of concave and convex shapes. The concave and convex shapes can be seen as dogbone- and barrel-shaped specimens in the laboratory, respectively.

The influence of the rock specimen profile on the mechanical behaviors of rocks has been studied by some researchers (Brace 1964; Brace et al. 1966; Mogi 1966; Nemat-Nasser and Horii 1982; Horii and Nemat-Nasser 1985). To further study the effect of specimen shape on rock failure, numerical uniaxial compressive tests were carried out on a dogbone-shaped and a barrel-shaped specimen. The parameters used in the simulations are based on these of Lac du Bonnet granite in the laboratory (Martin 1993), i.e., with an elastic modulus of 69 GPa, Poisson's ratio of 0.26, peak uniaxial compressive strength of 200 MPa, initial cohesion = 100 MPa and initial friction angle = 0°, peak tensile strength of 13.4 MPa, residual cohesion of 0.1 MPa, residual friction angle of 40° and residual tensile strength of 0 MPa. The models are built using FLAC^{3D} code, and the size is 50 mm in width and 100 mm in length (Fig. 9). A frictional buried joint,

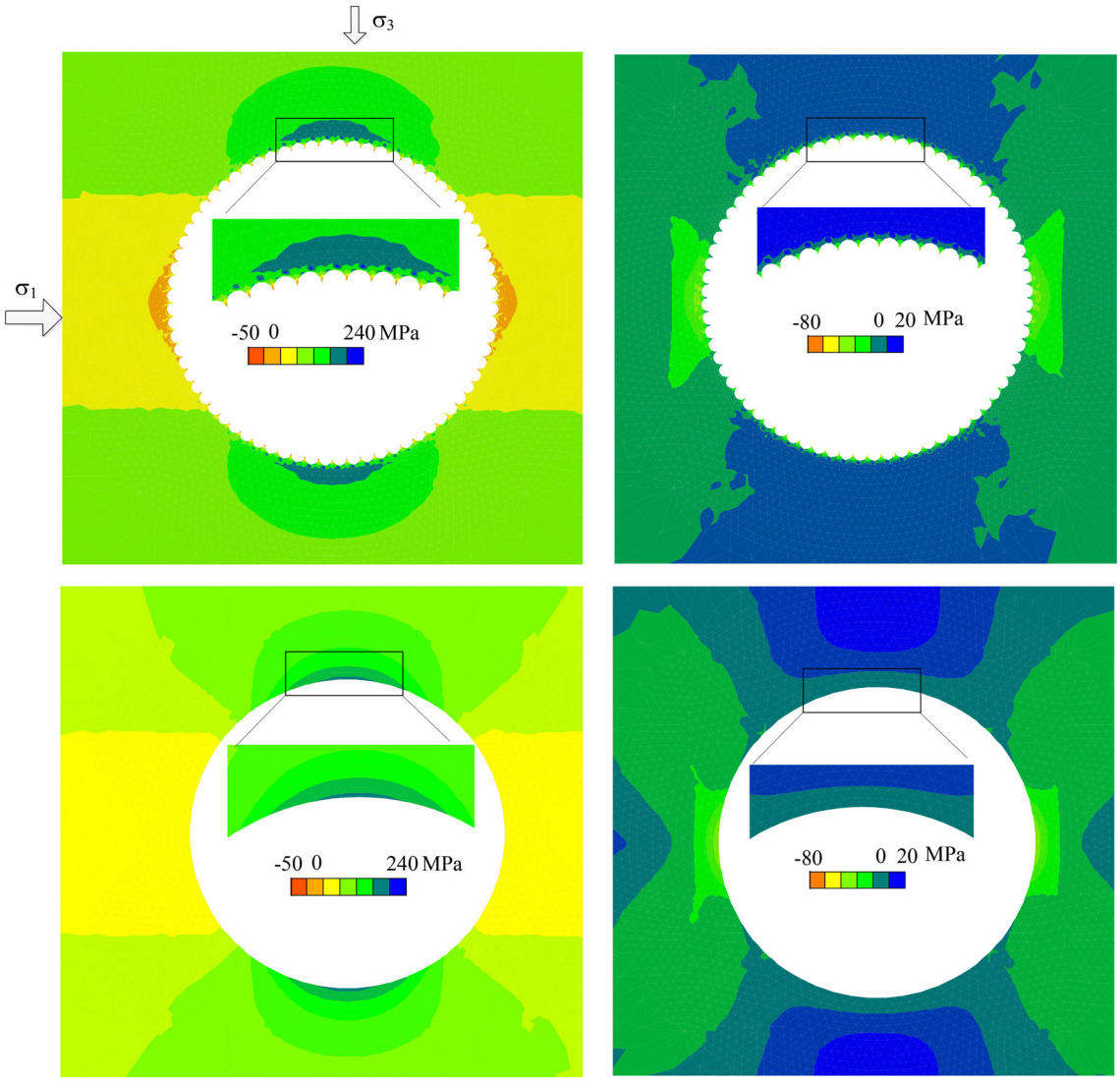

Fig. 8 The distribution of principal maximum and minimum stresses from elastic stress analysis. **a** Principal maximum stress, a/L =1; **b** principal minimum stress, $a/L = 1$; **c** principal maximum stress, $a/L = 0$; **d** principal minimum stress, $a/L = 0$

represented by the interface element in FLAC^{3D}, is built in the specimens. The friction angle and cohesion of the joint are 30° and 0 MPa, respectively. The length and orientation of the crack are 20 mm and 45° in both models.

A strain servo-control is used to conduct the numerical uniaxial compressive tests, and the results are shown in Fig. 9. When the load level defined by σ_1/UCS is low, i.e., σ_1/UCS <0.1, there is very little difference in fracture initiation and propagation between the two specimens, and the wing cracks grow as the load is increased. However, as the load is further increased, the fractures continue to grow in the barrel-shaped specimen, but the fracture growth is restricted in the dogbone-shaped specimen. It seems that lateral compression exists in the dogbone-shaped specimen and tension in the barrel-shaped specimen (Fig. 10). This is in agreement with the conclusions by Nemat-Nasser and Horii (1982) and Horii and Nemat-Nasser (1985), who carried out laboratory tests using the two shaped specimens.

Horii and Nemat-Nasser (1985) conducted a series of theoretical, experimental and numerical works to study the crack growth considering the lateral stress, crack direction, crack length, etc., and the relation between the axial stress and length of the propagated crack under various σ_3/σ_1 is shown in Fig. 11. It can be seen that even under a very small lateral confining stress, tension cracks emanating from the tips of the flaw grow to a finite length and then stop (Fig. 9); on the other hand, axial compression under very small lateral tension can cause the crack to grow in an unstable fashion, leading to axial splitting in the laboratory. The results are similar to what Hoek (1965) obtained.

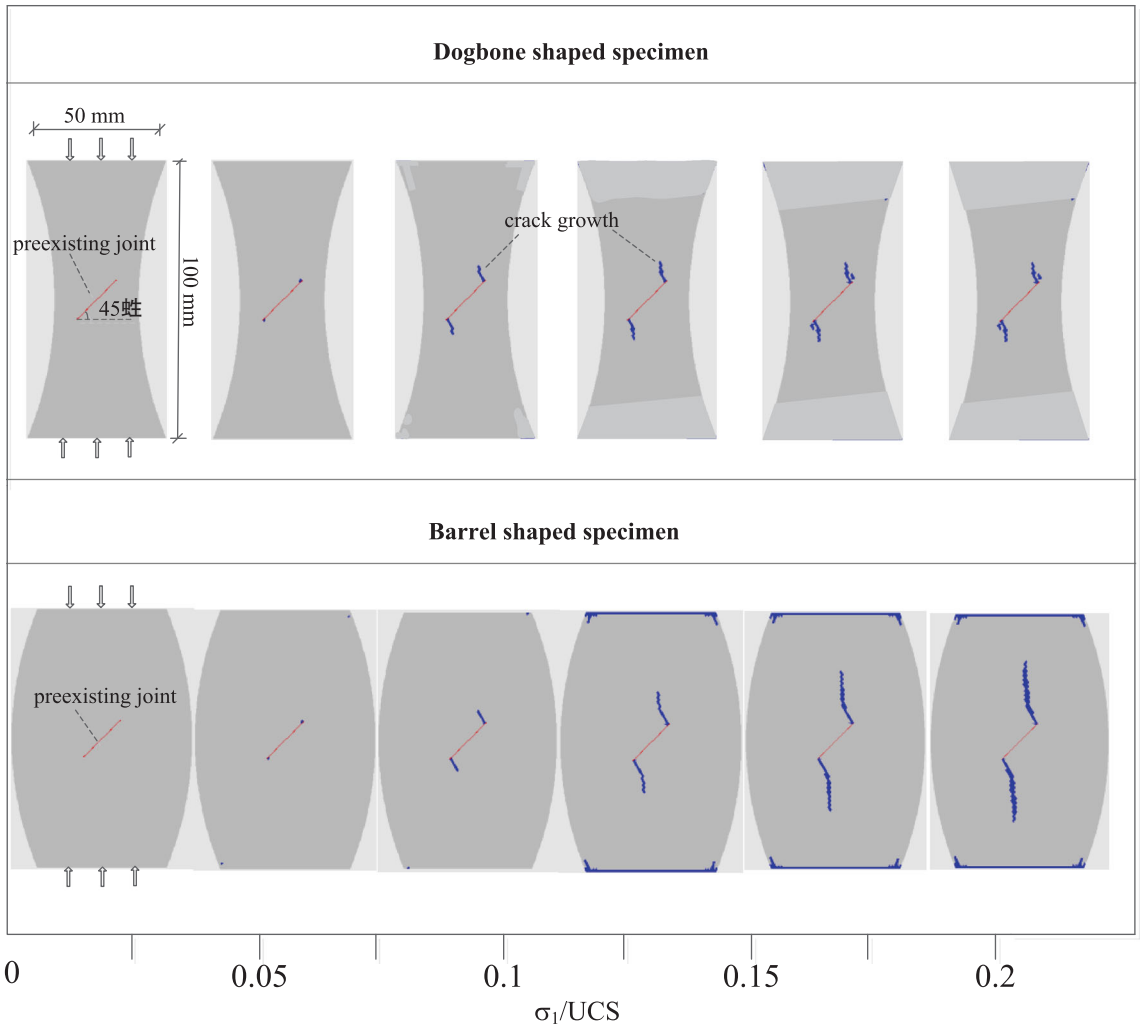

Fig. 9 The fracture initiation and propagation in a rock sample with a preexisting frictional joint under numerical uniaxial compressive tests

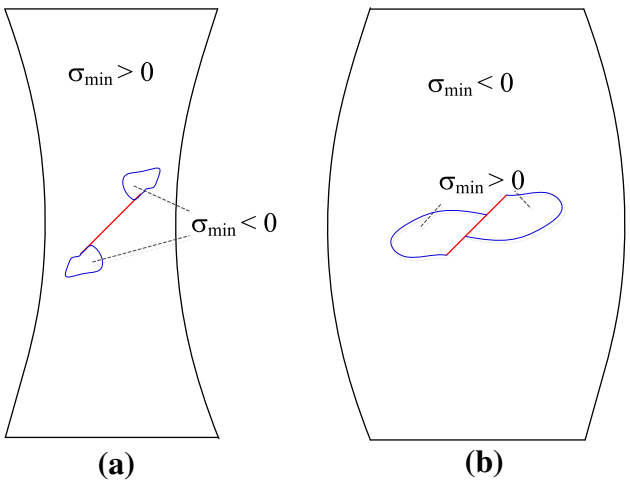

Fig. 10 The tensile and compressive stress distribution during compression. **a** Dogbone-shaped specimen; **b** barrel-shaped specimen

To summarize, the rough boundary caused the maximum principal stress (the tangential stress) to be concentrated, and the tensile stress occurred at the perimeter of the tunnel, making the failure take place more easily in the field, e.g., the Mine-by tunnel of URL (see Fig. 8). The boundary roughness effect on brittle failure cannot be ignored.

It should also be noted that the rock masses are massive and sparsely fractured in this study, and everything we discussed is based on this condition. Many publications show that the rock failures were observed in TBM tunnels with smooth boundaries, e.g., the rock burst occurring in the headrace tunnels in Jinping II hydropower station (Jiang et al. 2010; Gong et al. 2012). In these cases, different from what we discussed in this study, other factors play the key role in the brittle failure, such as the rock discontinuities and water flows.

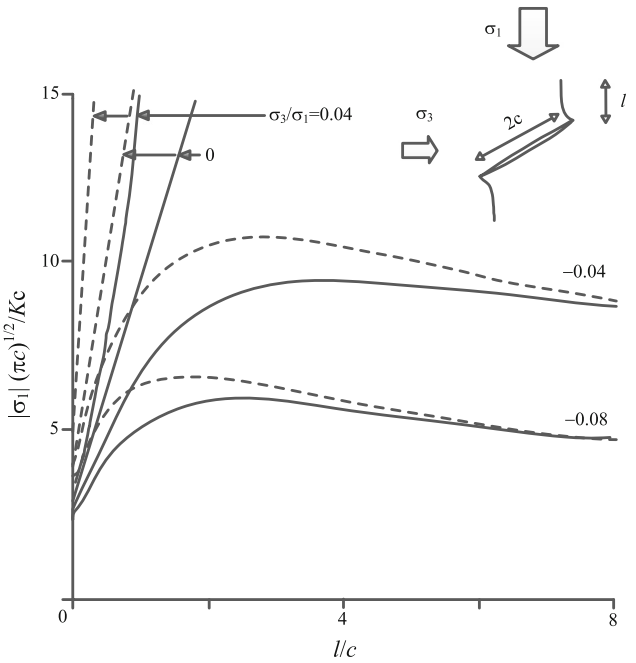

Fig. 11 Crack propagation under lateral compression stress or tensile stress [after Horii and Nemat-Nasser (1985)]

Conclusions

The in situ strengths of massive rock estimated by $UCS^{ci}_{field} = 0.45\ UCS_{lab}$ and $UCS^{cd}_{field} = 0.8\ UCS_{lab}$ were used to simulate brittle rock failure in two orthogonal tunnels at URL with as-built tunnel profiles. Brittle failure occurred in the tunnel aligned with the intermediate principal stress σ_2, but little failure was observed in the other tunnel aligned with the maximum principle stress σ_1. Two sets of model parameters were adopted in the numerical modeling, and the results were compared with the actual failure condition in the field. It is seen that strength given by the $UCS^{ci}_{field} = 0.45\ UCS_{lab}$ approach underestimates the in situ strength, and the strength given by $UCS^{cd}_{field} = 0.8\ UCS_{lab}$ approach predicts the rock failure observed underground better.

The roughness of the actual tunnel boundary can influence the local stress concentration, and this was numerically studied. It is indicated that both the maximum and minimum stresses around the tunnel perimeter are strongly affected by the roughness of the tunnel boundary. The maximum principal stress around the perimeter in the rough boundary model can be 1.4 times higher than that from the smooth boundary model. Another important observation is that tensile stress exists around the tunnel perimeter even in the areas where only compression stresses are expected if the smooth boundary model is used. This in turn can promote spalling failure in the so-called compression zones. It is suggested that more attention should be paid to the rock strength for $\sigma_3 < 0$ in the strength envelope.

Acknowledgments The work was financially supported by National Special Funds for Major State Basic Research Project under Grant No. 2010CB732001 and the National Science Foundation of China under grants nos. 41030749, 41322020 and 41172272. The authors also gratefully acknowledge financial support from the China Scholarship Council. Special thanks are given to Xin Wang, Jun Peng and Yuhang Xu for the advantageous discussions on rock failure.

References

Bieniawski ZT (1967) Mechanism of brittle fracture of rock: part I—theory of the fracture process. Int J Rock Mech Min Sci Abstr 4:395–406

Brace WF (1964) Brittle fracture of rocks. In: Judd AW (ed) State of stress in the Earth's crust. Elsevier, New York, pp 110–178

Brace WF, Paulding BW, Scholz CH (1966) Dilatancy in the fracture of crystalline rocks. J Geophys Res 71:3939–3953

Cai M (2011) Rock mass characterization and rock property variability considerations for tunnel and cavern design. Rock Mech Rock Eng 44:379–399

Cai M, Kaiser PK (2014) In-situ rock spalling strength near excavation boundaries. Rock Mech Rock Eng 47(2):1–17

Cai M, Kaiser PK, Tasaka Y, Maejima T, Morioka H, Minami M (2004) Generalized crack initiation and crack damage stress thresholds of brittle rock masses near underground excavations. Int J Rock Mech Min Sci 41:833–847

Diederichs MS (2007) The 2003 Canadian Geotechnical Colloquium: mechanistic interpretation and practical application of damage and spalling prediction criteria for deep tunnelling. Can Geotech J 44:1082–1116

Diederichs MS, Kaiser PK, Eberhardt E (2004) Damage initiation and propagation in hard rock during tunnelling and the influence of near-face stress rotation. Int J Rock Mech Min Sci 41:785–812

Eberhardt E (2001) Numerical modelling of three-dimension stress rotation ahead of an advancing tunnel face. Int J Rock Mech Min Sci 38:499–518

Eberhardt E, Stead D, Stimpson B (1999) Quantifying progressive pre-peak brittle fracture damage in rock during uniaxial compression. Int J Rock Mech Min Sci 36:361–380

Everitt RA, Brown A, Davison CC (1990) Regional and local setting of the underground research laboratory. In: Sinha RS (ed) Proceedings, international symposium on unique underground structures Denver, Vol 2. CSM Pewaa, Denver, Colo, pp 1–23

Fang Z, Harrison JP (2002) Development of a local degradation approach to the modelling of brittle fracture in heterogeneous rocks. Int J Rock Mech Min Sci 39(4):443–457

Gong QM, Yin LJ, Wu SY, Zhao J, Ting Y (2012) Rock burst and slabbing failure and its influence on TBM excavation at headrace tunnels in Jinping II hydropower station. Eng Geol 124:98–108

Guo SF, Qi SW, Zheng BW, Li XX (2013) The deformation and strength properties of Jinping marble with different confining pressures under cyclic loading—unloading tests. In: Proceedings of the international symposium and 9th asian regional conference of IAEG, global view of engineering geology and the environment, pp 413–417

Hajiabdolmajid V, Kaiser PK, Martin CD (2002) Modelling brittle failure of rock. Int J Rock Mech Min Sci 39:731–741

Hoek E (1965) Rock fracture under static stress conditions. In: National Mechanical Engineering Research Institute, Council for Scientific and Industrial Research

Hoek E, Brown ET (1980) Underground excavations in rock. London
Horii H, Nemat-Nasser S (1985) Compression-induced microcrack growth in brittle solids: axial splitting and shear failure. J Geophys Res 90:3105–3125
Jiang Q, Feng XT, Xiang TB, Su GS (2010) Rockburst characteristics and numerical simulation based on a new energy index: a case study of a tunnel at 2,500 m depth. B Eng Geol Environ 69:381–388
Kaiser PK, Diederichs MS, Martin CD, Sharp J, Steiner W (2000) Underground works in hard rock tunnelling and mining. In: Proceedings of the Geo Eng 2000, international conference on geotechnical and geological engineering. Technomic publishers, Melbourne, pp 841–926
Kaiser PK, Kim B, Bewick RP, Valley B (2011) Rock mass strength at depth and implications for pillar design. Mining Tech 120(3):170–179
Laigle F (2006) Short-term and delayed behaviors of underground openings—field observations and numerical simulations. In: Proceedings 4th international FLAC symposium. Madrid
Lockner DA (1995) Rock failure. AGU Reference Shelf 3:127–147
Lockner DA, Byerlee JD, Kuksenko V, Ponomarev A, Sidorin A (1992) Observations of quasistatic fault growth from acoustic emissions. Fault Mech Transp Prop Rocks 151:3–31
Martin CD (1990) Characterizing in situ stress domains at the AECL underground research laboratory. Can Geotech J 27:631–646
Martin CD (1993) The strength of massive Lac du Bonnet granite around underground openings: University of Manitoba
Martin CD (1997) Seventeenth Canadian Geotechnical Colloquium: the effect of cohesion loss and stress path on brittle rock strength. Can Geotech J 34:698–725
Martin CD, Chandler NA (1994) The progressive fracture of Lac du Bonnet granite. Int J Rock Mech Min Sci Abstr 31(6):643–659
Martin CD, Kaiser PK, McCreath DR (1999) Hoek-Brown parameters for predicting the depth of brittle failure around tunnels. Can Geotech J 36:136–151
Martin CD, Lu Y, Lan HX (2011) Scale effects in a synthetic rock mass. In: Qian QH, Zhou YX (eds) Harmonising rock engineering and the environment. Taylor and Francis Group, London, pp 257–258
Mogi K (1966) Some precise measurements of fracture strength of rocks under uniform compressive stress. Rock Mech Eng Geol 4:41–55
Nemat-Nasser S, Horii H (1982) Compression-induced nonplanar crack extension with application to splitting, exfoliation, and rockburst. J Geophys Res 87:6805–6821
Nicksiar M, Martin CD (2013) Crack initiation stress in low porosity crystalline and sedimentary rocks. Eng Geol 154:64–76
Read RS (2004) 20 years of excavation response studies at AECL's underground research laboratory. Int J Rock Mech Min Sci 41:1251–1275
Read RS, Chandler NA, Dzik EJ (1998) In situ strength criteria for tunnel design in highly-stressed rock masses. Int J Rock Mech Min Sci 35:261–278